Geophysical Research Letters

RESEARCH LETTER
10.1029/2024GL113926

Mars' Hemispheric Magnetic Field From a Full-Sphere Dynamo

C. Yan[1], A. Barik[2], S. Stanley[2,3], A. Mittelholz[4], A.-C. Plesa[5], and C.-L. Johnson[6,7]

[1]University of Texas at Austin, Institute for Geophysics, Austin, TX, USA, [2]Department of Earth and Planetary Sciences, The Johns Hopkins University, Baltimore, MD, USA, [3]The Johns Hopkins University Applied Physics Laboratory, Laurel, MD, USA, [4]Institute of Geophysics, Zurich, Switzerland, [5]German Aerospace Center (DLR), Institute of Planetary Research, Berlin, Germany, [6]Department of Earth, Ocean and Atmospheric Sciences, University of British Columbia, Vancouver, BC, Canada, [7]Planetary Science Institute, Tucson, AZ, USA

Key Points:

- We perform full-sphere numerical dynamo simulations to investigate the effects of thermal perturbations on the ancient martian dynamo
- We find hemispheric thermal perturbations at the core-mantle boundary lead to magnetic fields compatible with Mars' crustal magnetic hemisphericity
- Full-sphere dynamo models produce more hemispheric magnetic fields than dynamo models in spherical shells

Supporting Information:

Supporting Information may be found in the online version of this article.

Correspondence to:

C. Yan,
chi.yan@jsg.utexas.edu

Citation:

Yan, C., Barik, A., Stanley, S., Mittelholz, A., Plesa, A.-C., & Johnson, C.-L. (2025). Mars' hemispheric magnetic field from a full-sphere dynamo. *Geophysical Research Letters*, *52*, e2024GL113926. https://doi.org/10.1029/2024GL113926

Received 10 DEC 2024
Accepted 14 JAN 2025

Author Contributions:

Conceptualization: C. Yan, S. Stanley
Data curation: C. Yan
Formal analysis: C. Yan
Funding acquisition: S. Stanley
Investigation: C. Yan
Methodology: C. Yan, A. Barik
Project administration: S. Stanley
Resources: S. Stanley, A. Mittelholz, C.-L. Johnson
Software: A. Barik
Supervision: S. Stanley, C.-L. Johnson
Validation: C. Yan
Visualization: C. Yan, A. Barik
Writing – original draft: C. Yan
Writing – review & editing: C. Yan, A. Barik, S. Stanley, A. Mittelholz, A.-C. Plesa, C.-L. Johnson

Abstract Seismic measurements from the NASA Mars InSight mission revealed that Mars' core has a relatively low density, implying a larger fraction of lighter elements than previously thought, which further leads to a low melting temperature. Thus, Mars probably never developed a solid inner core during its early history when the dynamo was active. We perform full-sphere dynamo simulations to eliminate the influence of an inner core on dynamo behaviors and investigate how various magnitudes of heat flux perturbations at the core-mantle boundary affect the field morphology, comparing results to those from models with small inner cores. We find that a hemispheric magnetic field can result when the heat flux is concentrated in one hemisphere. Moreover, a dynamo model without the presence of an inner core can better explain Mars' crustal magnetic field dichotomy than that in a spherical shell surrounding a solid inner core.

Plain Language Summary Recent measurements from the NASA Mars InSight mission show that Mars' core is less dense than we previously believed. This indicates that Mars probably never developed a solid inner core in the earliest times in its history. Here we conducted simulations to understand the effects of this lack of a solid inner core. We find that the lack of an inner core can better explain the north-south dichotomy of Mars' observed magnetic field.

1. Introduction

Although the red planet, Mars, lacks a present-day intrinsic magnetic field, the existence of crustal magnetic fields suggests a dynamo was once active in its early history. Mars' crustal magnetic field was first discovered by the Mars Global Surveyor (MGS) mission in 1997 (Acuna et al., 1999). The crustal magnetic field was subsequently mapped by the Mars Atmosphere and Volatile EvolutioN (MAVEN) mission (Jakosky et al., 2015) and measured at the surface of Mars by the Interior Exploration using Seismic Investigation, Geodesy and Heat Transport (InSight) mission (Banerdt et al., 2020; Johnson et al., 2020). The presence of a global magnetic field affects atmospheric escape channels and thus the planet's ability to retain its atmosphere (Dehant et al., 2007; Jakosky & Phillips, 2001). Understanding Mars' ancient dynamo therefore places important constraints on atmospheric loss mechanisms and Mars' early climate evolution.

The timing of the ancient martian dynamo can currently be inferred from observations of the crustal magnetic field on Mars and the paleomagnetic record of Mars' meteorites. An early dynamo was first hypothesized from the crustal field record of the MGS mission (Acuna et al., 1999), and the lack of magnetic field signatures above the large basins (Lillis et al., 2013; Vervelidou et al., 2017), Hellas, Utopia, Isidis, and Argyre was interpreted as a sign of ceased dynamo at the time of their formation around 4.1 Ga (Mittelholz & Johnson, 2022, and references therein). While age dating of the magnetized martian meteorite ALH 84001 was consistent with this assessment (Weiss et al., 2002), some studies suggested a young dynamo that operated after the emplacement of the basins (e.g., Langlais & Purucker, 2007; Milbury et al., 2012).

More recently, analysis of a higher spatial resolution crustal magnetic field data model (Mittelholz et al., 2020) and paleomagnetic investigations of inclusion of ALH 84001 (Steele et al., 2023) indicate a dynamo that operated before and after the time of the basins' formation. Furthermore, several explanations regarding the small magnetic field amplitudes in the basin interior have been proposed. These include a reversing dynamo (Steele et al., 2022)

or excavation as a result of the impact (Mittelholz et al., 2023). Consequently, the latest interpretation of dynamo timing supports the existence of a long-lived, potentially reversing dynamo up to at least 3.7 Ga.

Tidal and seismic studies from InSight measurements suggest the presence of substantial amounts of light elements in Mars' liquid core (Khan et al., 2022; Terasaki et al., 2019) and the absence of a solid inner core (Konopliv et al., 2020; Stähler et al., 2021). Core-transiting seismic phases detected in InSight seismic data (Irving et al., 2023) have enabled further constraints on the size of the outer core and core diffracted phases identified in an impact event attribute part of the light elements to the possible existence of a molten silicate, basal magma layer above the core mantle boundary (CMB) (Khan et al., 2023; Samuel et al., 2023). This further indicates that Mars' core may not have cooled sufficiently to meet the eutectic melting temperatures at Mars' core conditions. Without compositional buoyancy provided by core crystallization, it becomes challenging to power a dynamo for more than ∼500 million years. However, low thermal conductivity measured on sulfur-rich iron alloys (Pommier, 2018; Pommier et al., 2020) may enable a longer-lived thermally driven dynamo than previously thought (Greenwood et al., 2021).

One of the most distinctive features of Mars' crustal magnetic field is its uneven distribution in the northern and southern hemispheres (Figure S1 in Supporting Information S1). The strongest crustal magnetic fields are found in regions around Terra Cimmeria and Terra Sirenum in the southern hemisphere, whereas only weak magnetic fields are observed in the northern hemisphere. Furthermore, no significant magnetic fields can be identified in either large impact basins (e.g., Isidis and Utopia in the northern hemisphere, Hellas and Argyre in the southern hemisphere) or large volcanic provinces (e.g., Tharsis and Elysium, Johnson & Phillips, 2005). Various hypotheses have been proposed to explain the observed dichotomy in Mars' crustal magnetic field, ranging from post-dynamo crustal modification processes such as impact demagnetization (e.g., Andrews-Hanna et al., 2008; Mohit & Arkani-Hamed, 2004; Nimmo & Gilmore, 2001), hydrothermal circulation (e.g., Ojha et al., 2021; Quesnel et al., 2009; Solomon et al., 2005), to hemispheric dynamo action (e.g., Amit et al., 2011; Stanley et al., 2008). Our present study focuses on the last mechanism.

Most of the hemispheric dynamo explanations rely on hemispheric thermal perturbations at the CMB. Endogenic processes such as mantle circulation (e.g., Elkins-Tanton et al., 2003, 2005; Ke & Solomatov, 2006; J. H. Roberts & Zhong, 2006; Zhong & Zuber, 2001) or exogenic processes such as impact heating (e.g., Frey & Schultz, 1988; Nimmo et al., 2008; Wilhelms & Squyres, 1984) could result in hemispheric thermal perturbations in the mantle, causing higher heat fluxes out of the core in the southern hemisphere compared to the northern hemisphere (Figure S2a in Supporting Information S1). This hemispheric heat flux perturbation could lead to a dynamo operating predominantly in the southern hemisphere, generating significantly stronger magnetic fields in that region. Prior research has investigated hemispheric dynamo models with the preferential hemispheric heat flux perturbations at the CMB (e.g., Amit et al., 2011; Dietrich & Wicht, 2013; Stanley et al., 2008; Yan et al., 2023). However, these dynamo models were all performed in spherical shell geometries, where a sizable solid inner core, like the case for the present-day Earth, is assumed. However, this geometry would not accurately represent Mars' dynamo region if Mars lacked a solid inner core throughout its dynamo history. In such a scenario, a full-sphere is more suitable to simulate Mars' core geometry.

The presence or absence of a solid inner core has significant influence on core dynamics. First, the presence of a solid inner core leads to extra buoyancy sources near the inner core boundary (ICB), that is, the latent heat produced and the light elements released when iron or iron alloys solidify at the ICB. The absence of an inner core suggests the lack of these buoyancy sources associated with the inner core growth. Second, in the presence of a solid inner core, flows tend to organize into separate regions inside and outside of the cylindrical region tangent to the inner core at the equator, known as the tangent cylinder (TC).

The presence or absence of a solid inner core also affects the subsequent dynamo behavior. For example, the existence of a solid inner core has been proposed to stabilize the magnetic field against reversals through magnetic inertia due to the long diffusion time in the inner core (Gubbins, 1999). Interestingly, various pieces of evidence including paleopole reconstruction from magnetic anomalies (e.g., Milbury et al., 2012; Thomas et al., 2018) and paleomagnetic signatures of the martian meteorite ALH84001 (Steele et al., 2023) indicate Mars' ancient magnetic field may have undergone reversals in its history. Additionally, dynamo simulations show that magnetic fields are distinctively different inside and outside the TC (Schaeffer et al., 2018). Therefore, the resulting dynamo behavior and the magnetic field morphology are expected to be different if Mars does not possess a solid inner core and thus a TC.

Dynamo models in a full-sphere geometry have been employed to simulate the ancient geodynamo prior to inner core nucleation (Landeau et al., 2017), hemispheric dynamos in stellar context (Benjamin et al., 2020), dynamics induced by mechanical forcings (Cébron et al., 2021; Lin et al., 2016) or double diffusive convection (Monville et al., 2019). It is worth noting that hemispheric magnetic fields can also be produced without specific heat flow patterns, but by invoking the equatorially antisymmetric, axisymmetric (EAA) flow modes in a limited parameter regime, either in a full-sphere geometry (Landeau & Aubert, 2011) or in spherical shells (Wu et al., 2024). However, allowing CMB lateral heat flux perturbations may significantly broaden this parameter regime. It is not yet clear how heat flux perturbations in full-sphere dynamos affect the internal dynamics and the resulting magnetic field morphology observable at the surface. It is therefore essential to evaluate Mars' ancient dynamo in a full-sphere geometry to properly account for the absence of a solid inner core.

In the present study, we investigate Mars' ancient dynamo through 3D numerical dynamo simulations that are performed in a full-sphere geometry and evaluate the effects of hemispheric heat flux perturbations at the CMB on the resulting magnetic field morphology. The rest of the paper is organized as follows: Section 2 contains details of the numerical methods, Section 3 describes the results, Section 4 contains a discussion, and the paper ends with conclusions in Section 5.

2. Methods

We study Mars' ancient dynamo by simulating dynamo action in a rapidly rotating sphere, using the 3D magnetohydrodynamic code MagIC (Schaeffer, 2013; Wicht, 2002), to explore the effects of hemispheric heat flux perturbations on the resulting magnetic field morphology. We adopt the Boussinesq approximation in our dynamo models, where density variations are only considered in the buoyancy term. This is justified given that the background density variation within Mars' core is sufficiently small. The code MagIC has been benchmarked against Christensen et al. (2001) and the full-sphere dynamo benchmark of Marti et al. (2014). Further details about the non-dimensional parameters and model equations can be found in Supporting Information S1.

For full-sphere dynamo models, boundary conditions are required only at the CMB, where we assume a stress-free CMB with a fixed heat flux boundary condition. The region outside the CMB (the mantle) is assumed to be electrically insulating by enforcing a potential field boundary condition on the magnetic field. The heat flowing out of the CMB is balanced by the heat generated within the fluid core volume through a presumed uniform volumetric heat source ϵ summing over the internal heating and secular cooling, that is,

$$Q_{CMB} = P_r \frac{4}{3}\pi r_0^3 \epsilon, \tag{1}$$

where P_r is the Prandtl number defined in Supporting Information S1. We then further incorporate a zonal, degree-one spherical harmonic pattern Y_1^0 superimposed on a homogeneous Y_0^0 CMB heat flux background to examine the influence of Mars' lower mantle thermal heterogeneity on dynamo action. With the Y_1^0 variable heat flux (VHF) perturbations, minimum and maximum heat fluxes are expected out of the northern and southern hemispheres at the CMB, respectively (Figure S2b in Supporting Information S1). We vary the strength of the heat flux perturbations at the CMB through $|\Delta q|_{\max}$, which represents the maximum difference in heat flux perturbation at the CMB. This can be connected to q^* as defined in Amit et al. (2011) by $|\Delta q|_{\max} = 0.58q^*$. The maximum heat flux perturbation is about 87% of the mean heat flux at the CMB, not to be scaled to dimensional values due to the unrealistically high viscous forces assumed in the dynamo models.

We employ spectral methods using 97 Chebyshev polynomials in the radial direction. Scalars on each spherical surface are resolved in latitude and longitude using spherical harmonics, with a maximum degree $L_{\max} = 213$ at the CMB (i.e., $r = 1$) and minimum degree $L_{\min} = 1$ at the sphere's center (i.e., $r = 0$). The local maximum degree of the spherical harmonic expansion varies with the radius, following Marti et al. (2014), to prevent numerical instabilities near the sphere's center, specifically, $l_{\max}(r) = 1 + (L_{\max} - 1)(r/r_0)^{\frac{1}{2}}$ (Monville et al., 2019). Each dynamo simulation is run for several viscous diffusion times and is allowed to reach equilibrium. Time-averaged values denote those averaged over the full duration of the simulation once the dynamo models are equilibrated. Table 1 presents the input and the diagnostic parameters for our simulations.

Table 1
Non-Dimensional and Time-Averaged Diagnostic Parameters of Full-Sphere (1–9) and Spherical Shell (10–12, Yan et al. (2023)) Dynamo Simulations

Model	$\lvert\Delta q\rvert_{\max}$	Tilt(°)	f_{dip}	E_{pol}/E_{tor}	H_{sur}	Rev. freq
1	0	5.3 ± 2.8	0.52 ± 0.06	0.96	1.02 ± 0.06	–
2	0.05	6.5 ± 3.6	0.48 ± 0.07	0.90	1.08 ± 0.08	–
3	0.1	7.7 ± 4.4	0.41 ± 0.08	0.77	1.18 ± 0.08	–
4	0.15	10.4 ± 4.4	0.27 ± 0.07	0.49	1.35 ± 0.12	–
5	0.2	12.2 ± 7.6	0.22 ± 0.04	0.34	1.44 ± 0.23	–
6	0.3	15.0 ± 6.5	0.15 ± 0.05	0.27	1.59 ± 0.20	–
7	0.35	67.2 ± 69.8	0.10 ± 0.04	0.24	1.74 ± 0.32	2.5
8	0.4	102.6 ± 72.0	0.08 ± 0.04	0.18	1.82 ± 0.5	5.7
9	0.5	101.5 ± 69.2	0.07 ± 0.03	0.15	1.98 ± 0.49	10
10	0	4.7 ± 1.9	0.79 ± 0.04	1.21	0.99 ± 0.04	–
11	0.5	10.7 ± 6.7	0.37 ± 0.14	0.14	1.34 ± 0.19	–
12	1.0	80.90 ± 51.92	0.06 ± 0.06	0.33	1.64 ± 0.68	10

Note. The dipole tilt is calculated by averaging the tilt over the full duration of the models once they have reached equilibrium. Dipolarity f_{dip} is the relative dipole strength defined as the ratio on the outer boundary that is, the core-mantle boundary of the magnetic energy in the axisymmetric dipole to the magnetic energy in spherical harmonic degrees l 1 to 11. E_{pol}/E_{tor} is the ratio of the poloidal to the toroidal magnetic energy (see SI for more information, R. Roberts, 2007) of the RMS field in the fluid outer core. H_{sur} gives the hemispheric dichotomy ratio averaged over snapshots taken at various times over the full duration of models once they have reached equilibrium (see Equation 2). "Rev. freq" gives the number of reversals per viscous diffusion time if the magnetic dipole field is reversing. Other non-dimensional parameters: Rayleigh, Ekman, Prandtl, and magnetic Prandtl numbers, are held fixed at $Ra = 4.0 \times 10^8$, $E = 3.0 \times 10^{-5}$, Pr = 1 and $Pm = 5$ for full-sphere models (1–9) and $Ra = 2.3 \times 10^7$, $E = 9.5 \times 10^{-5}$, Pr = 1, and $Pm = 1$ for spherical-shell models (10–12).

For comparison, we also run spherical shell models assuming an Earth-like solid inner core (i.e., the inner core to outer core ratio is 0.35). Both the inner core and core mantle boundaries are stress-free, electrically insulating, and have fixed heat flux boundary conditions. The spherical shell dynamos are also internally heated to eliminate effects of heating sources related to inner-core growth such as expulsion of light elements and latent heat released at the ICB (Yan et al., 2023). It is worth emphasizing that the non-dimensional parameters sampled in this study are different for full-sphere and spherical shell dynamo models (see Table 1). This is because dynamo models with varying geometries essentially operate in different parameter spaces. In this study, we focus on models in a parameter space based on the magnetic field morphology of the control models, that when homogeneously heated, produce non-reversing, dipolar dominated fields for both full-sphere and spherical shell models. The homogeneously heated spherical shell control models were selected based on the model with the highest Rayleigh number that still produce a dipole-dominated field. We then add hemispheric heat flux perturbations at the CMB onto the dynamo models and examine the resulting effects on the magnetic field behavior.

3. Results

We first investigate our full-sphere dynamo simulations with a homogeneous heat flux boundary at the CMB (i.e., model 1 in Table 1) and compare it to a homogeneously heated model with a solid inner core (i.e., model 10 in Table 1). Both models produce dipole dominated magnetic fields (see Figures 1a and 1b) that are non-reversing. However, the characteristics of the flow dynamics are different in the two models. Due to the absence of the solid inner core, there are no downwellings along the TC at high latitudes or large-scale upwellings at the equator (Figure 1e), which are characteristic flow features in spherical shell dynamos (Figure 1f). Furthermore, the convective cells in the full-sphere model can extend from one hemisphere to the other, without the obstruction caused by the ICB (Figure 1e).

To investigate the influence of hemispheric thermal perturbations on the full-sphere dynamo, we then introduce VHF perturbations of varying magnitudes (i.e., models 2–9 in Table 1) to the full-sphere model. We find that the

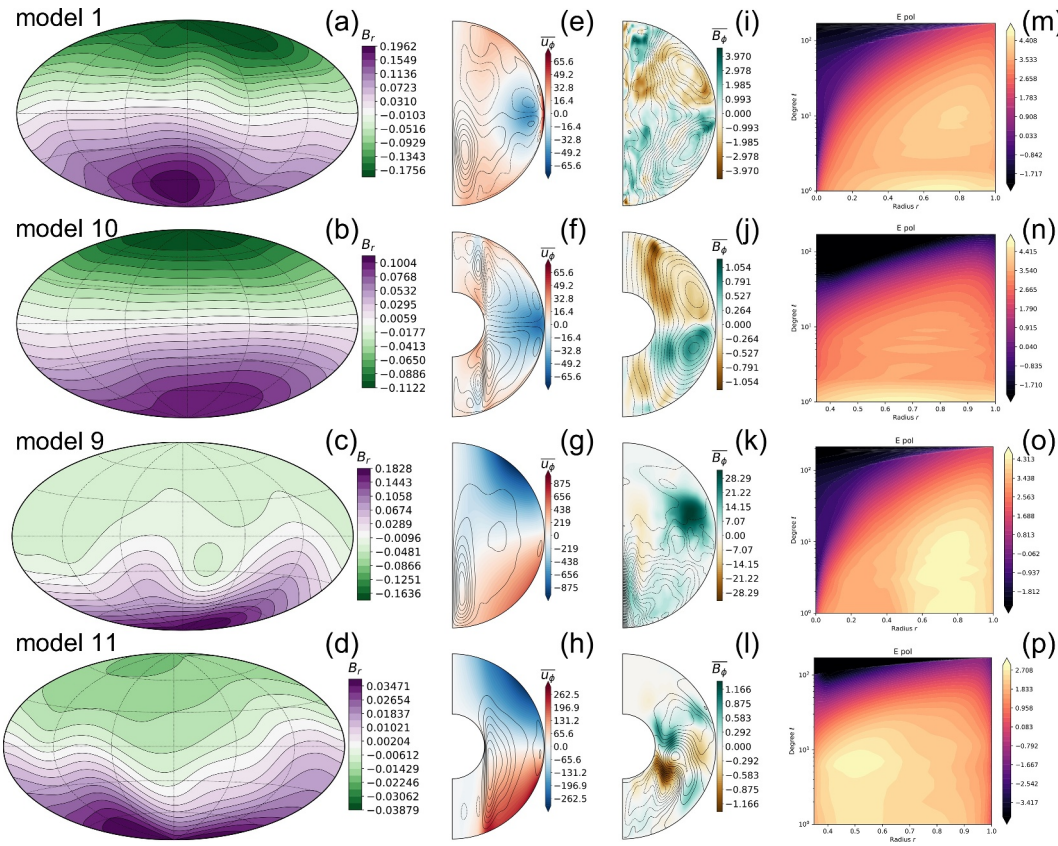

Figure 1. Comparison of magnetic and velocity fields for full-sphere (models 1 and 9) and spherical shell (models 10 and 11) dynamo models with homogeneous (rows 1–2) and hemispheric (rows 3–4) heat flux perturbations at the CMB. Panels (a) to (d) show snapshots of the radial magnetic field extrapolated to the surface, while panels (e) to (h) display the time-averaged axisymmetric velocity fields, with filled blue (red) contours representing retrograde (prograde) azimuthal flows and (dashed) solid streamlines represent (counter)-clockwise meridional circulation. Panels (i) to (l) show the axisymmetric toroidal (filled contours, $\overline{B_\phi}$) and poloidal (streamlines) magnetic fields. Panels (m) to (p) show the time-averaged poloidal magnetic energy spectra distribution in the outer core on a logarithmic scale, where values in the color bar represent the base-10 logarithmic values of the magnetic energy. Units are non-dimensional.

resulting magnetic field becomes increasingly hemispheric with increasing $|\Delta q|_{\max}$ for models in both full-sphere and spherical shell geometries as the magnetic field concentrates in the southern hemisphere (see Figures 1c and 1d). The meridional circulation is mostly constrained to the southern hemisphere due to a higher thermal forcing from the larger heat flux in the south (Figure 1g). Furthermore, the poloidal flows are mostly concentrated along the rotation axis in the full-sphere dynamo model 9 (Figure 1g), but in the spherical shell model 11 they are nested close to the TC (Figure 1h). The zonal flows invoked by the hemispheric VHF perturbation at the CMB are overall anti-symmetric about the equator with the northern (southern) hemisphere being dominated by retrograde (prograde) flows (Figures 1g and 1h), demonstrating EAA mode excitation (see more details in Supporting Information S1). However, for a spherical shell, these zonal flows are limited to regions outside the TC.

As demonstrated in Figure 2a, full-sphere dynamo models present a systematic trend in magnetic energy components as we gradually increase the magnitude of the hemispheric heat flux perturbations. First of all, the homogeneously heated dynamo (i.e., model 1, $|\Delta q|_{\max} = 0$) has a time and volume-averaged magnetic energy which is equally partitioned between the poloidal and toroidal parts $\left(E_{pol}/E_{tor} \sim 0.96\right)$. As the $|\Delta q|_{\max}$ increases, the total magnetic energy increases until reaching a plateau about 3 times higher than model 1, at $|\Delta q|_{\max} = 0.2$, whereas the ratio of the poloidal-to-toroidal magnetic energy steadily decreases to a minimum of 0.15 at the largest $|\Delta q|_{\max}$ of 0.5 in our full-sphere models. Additionally, the dipolarity f_{dip} of the full-sphere dynamo models decreases as the magnitude of the hemispheric heat flux perturbations $|\Delta q|_{\max}$ increases.

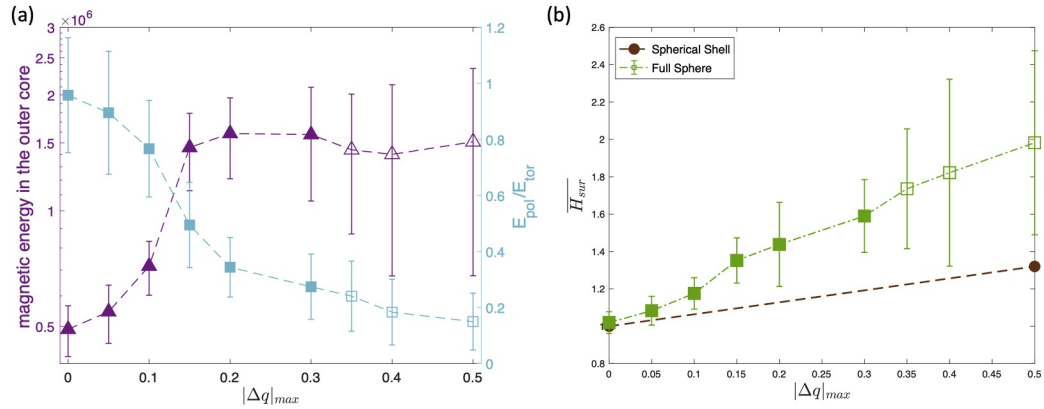

Figure 2. (a) The time-averaged total (purple triangles) and the ratio of the poloidal to toroidal (blue squares) magnetic energy integrated in the outer core as a function of the $|\Delta q|_{\max}$ for full sphere models. (b) The time-averaged magnetic hemisphericity ratio $\overline{H_{sur}}$ at varying magnitudes of $|\Delta q|_{\max}$ for full sphere (green squares) and spherical shell (brown circles) models. (Filled) Open symbols represent (non-)reversing dynamos.

To evaluate the level of hemisphericity of magnetic fields in our dynamo models, we calculate the ratio of the time-averaged RMS magnetic field strengths at the planetary surface in the southern and northern hemispheres (H_{sur}):

$$H_{\text{sur}} = \left[\frac{\int_0^{2\pi}\int_{\pi/2}^{\pi}\vec{B}^2\sin\theta d\theta d\phi}{\int_0^{2\pi}\int_0^{\pi/2}\vec{B}^2\sin\theta d\theta d\phi}\right]^{1/2} \quad (2)$$

where θ and ϕ are colatitude and longitude respectively, and the magnetic field $\vec{B}$ is evaluated at the surface of Mars (r_S) by upward continuing the magnetic field from the CMB (r_0) to the surface using $r_0/r_S = 0.54$, where $r_0 = 1830$ km from Stähler et al. (2021). The slightly smaller ratio of ($r_0/r_S = 0.53$) based on the recently suggested core radius of Mars (1795 ± 15 km, Irving et al., 2023) does not change our results significantly.

Figure 2b demonstrates the overall increasing trend of the hemisphericity H_{sur} with the increasing $|\Delta q|_{\max}$ at the CMB in full-sphere dynamo models. At relatively small $|\Delta q|_{\max}$ (0–0.3), the resulting magnetic field is non-reversing and dipole dominated, with a low standard deviation owing to a low time variability of the magnetic field morphology. These fluctuations become stronger as $|\Delta q|_{\max}$ increases. When $|\Delta q|_{\max}$ reaches a critical value of 0.35, the resulting magnetic field transitions into a reversing, non-dipolar regime. Figure S3 in Supporting Information S1 presents an example of a reversing hemispheric dynamo model where the dipole tilt angle is aperiodically reversing. The magnetic fields are nevertheless more concentrated in the southern hemisphere as $H_{sur} > 1$ at all times, except during the event of a dipole reversal (e.g., at $t = 1.77$ in Figure S3 in Supporting Information S1) where H_{sur} can be temporarily smaller than unity. In the reversing, multipolar regime, the resulting magnetic hemisphericity also increases with increasing $|\Delta q|_{\max}$. Furthermore, the hemisphericity values become more variable in time than models with relatively smaller $|\Delta q|_{\max}$ (Figure 2b), due to increased time variability of the field in the southern hemisphere and relatively low hemisphericity values during periods of reversals.

Interestingly, we find that full-sphere dynamos are more hemispheric than spherical shell models with the same $|\Delta q|_{\max}$. To achieve similar levels of hemisphericity (e.g., $H_{sur} \sim 1.3$), the required $|\Delta q|_{\max}$ in full-sphere dynamo models (0.15) is more than three times smaller than spherical shell dynamo models (0.5). Furthermore, at the same $|\Delta q|_{\max}$ (e.g., of 0.5), the resulting H_{sur} in full-sphere models (1.98) is considerably higher than that in spherical shell models (1.32).

Full-sphere and spherical shell dynamo models produce magnetic fields concentrated in distinct regions. The magnetic energy in full-sphere dynamos is predominantly in the outer part of the core, ranging from $r = 0.6$ to 0.8 (Figure 1o). This is also observable in Figure 1k, where the poloidal magnetic field is strong near the south pole along the rotation axis. Conversely, spherical shell dynamos tend to produce magnetic fields clustered around the

TC, from $r = 0.4$ to 0.6, situated much deeper within the core than full-sphere models (Figure 1p). Moreover, magnetic fields produced by full-sphere dynamos are much stronger than those by spherical shell dynamo models (Figures 1k and 1l). Consequently, when extrapolated to the surface, magnetic fields in the southern hemisphere are stronger in the full-sphere models than those in spherical shell models. Given similar minimal fields produced in the northern hemisphere, this leads to a higher hemisphericity value in full-sphere dynamos. Similar effects were reported in Landeau et al. (2017), where magnetic fields are concentrated comparatively deep (shallow) in full-sphere (spherical shell) models. However, the mechanisms in our models likely differ from Landeau et al. (2017) due to the different heating sources. The spherical shell models in Landeau et al. (2017) are heated at the ICB so buoyancy is concentrated near the ICB, whereas our spherical shell models feature internal heating so that buoyancy is distributed throughout the core. Therefore this difference of magnetic field concentration is more likely caused by geometries than the buoyancy force in our study. We also observe manifested EAA flow modes in our hemispheric dynamo models (Figures 1g and 1h), more detailed discussion can be found in the Supporting Information S1.

To compare our simulation results with Mars' surface magnetic field, we have scaled the modeled field to physical values using the following parameters: core density ρ of $6 \times 10^3 \mathrm{kg/m^3}$ (Stähler et al., 2021), planetary rotation rate Ω of $1.13 \times 10^{-6} \mathrm{s^{-1}}$, and magnetic diffusivity λ of $2 \mathrm{m^2/s}$. This scaling leads to a modeled surface magnetic field of 24 $\mu\mathbf{T}$, consistent with the paleointensities from Steele et al. (2023), and the suggestion in Mittelholz et al. (2020) that the ancient martian field strength was Earth-like. For more recent studies (Khan et al., 2023; Samuel et al., 2023) where the core size is significantly smaller and assuming that the core cooling is not restricted by the molten silicate layer, the modeled magnetic field extrapolated to the surface decreases to $\sim$**14** $\mu\mathbf{T}$, as the magnetic field decreases exponentially with the ratio r_0/r_S away from the dynamo source region. However, further investigation is necessary to determine if this trend continues as simulation parameters approach asymptotic values close to that of Mars.

4. Discussion

The strength of the crustal magnetic field and the resulting hemisphericity at the surface depends on various geological features according to their cooling times. For extrusive geological features such as volcanos or lava flows, the time required for these crustal rocks to cool below their Curie temperatures is instantaneous, typically on the order of days to a few years, compared to the timescales on which magnetic fields evolve. For example, the magnetization of volcanic flows in Lucus Planum on Mars has been identified (Mittelholz et al., 2020) and confirmed as pyroclastic in origin (Ojha & Mittelholz, 2023). In such scenarios, the magnetic field is captured in individual snapshots. In the reversing full-sphere model 9, the majority of magnetic hemisphericity values measured across various instances are around 2, smaller than the lower bound of Mars' magnetic dichotomy ratio ($2.35 - 4.7$; Amit et al., 2011; Langlais et al., 2019). But there are a few instances in our full-sphere models that produce a magnetic hemisphericity ratio (e.g., $H_{sur}(\max) = 3.32$ in model 9) at the surface that is compatible with the observed Mars' crustal magnetic field dichotomy ratio.

Conversely, the cooling time for intrusive geological features and large impact basins is significantly longer compared to extrusive ones. Depending on the size of the intrusion, the duration can vary widely. In such instances, if the magnetic field's reversing period is shorter than the cooling time, the rocks might record the time-varying magnetic fields during the cooling process, resulting in a net crustal magnetic field that is time-averaged at the surface (Rochette, 2006; Steele et al., 2022). Smaller intrusions, such as narrow dikes, cool on a timescale of a few thousand years—a duration comparable to the reversing period in our full-sphere dynamo models. Interestingly, if the magnetic field's time average is taken during reversals, the resulting time-averaged field is often highly concentrated in the southern hemisphere, yielding a more hemispheric field than individual snapshots during the reversal event. Figure S4 in Supporting Information S1 presents a few examples of the time-averaged magnetic fields in both full-sphere and spherical shell models, with the highest hemisphericity ratio $H_{sur} = 4.28$. This suggests that the magnetic field in the northern hemisphere may cancel out to a larger extent compared to those in the southern hemisphere during a reversal event, providing a resulting time-averaged magnetic field that is even more hemispheric. However, as demonstrated in Figure S4e in Supporting Information S1, if the magnetic field is averaged over a significantly larger number of reversals, the resulting time-averaged field, although it may still exhibit a hemispheric pattern, could become too weak to be effectively recorded.

In addition, our study of full-sphere dynamo models carries substantial implications for geodynamo models prior to inner core nucleation. For instance, it is essential to reassess the effects of various external or internal thermal perturbations on the paleomagnetic field. Notably, in a full-sphere dynamo context, these heat flux perturbations could potentially exert stronger influences on the magnetic field morphology.

Future work is needed to systematically explore full-sphere dynamo models as they asymptotically approach planet-like parameters and investigate their properties, such as the transition from dipolar-dominated fields to multipolar fields. Additionally, scaling laws relating characteristic properties to control parameters for full-sphere dynamo simulations need to be derived and compared against those for spherical-shell dynamos.

5. Conclusion

Our study demonstrates that full-sphere dynamo models, aligning closely with the current understanding of Mars' core structures, are capable of generating hemispheric magnetic fields predominantly in the southern hemisphere, with preferential hemispheric heat flux perturbations at the CMB. Specifically, with higher heat flux perturbation, the full-sphere dynamo models enter the reversing regime, and produce magnetic fields with highest degrees of hemisphericity. Compared to conventional spherical shell dynamo models, the full-sphere geometry is more advantageous for producing hemispheric magnetic fields. In conclusion, incorporating the latest findings from the InSight mission into our examination of Mars' core dynamo offers a stronger explanation for the planet's crustal magnetic field.

Data Availability Statement

The numerical dynamo code MagIC is open source and available at https://magic-sph.github.io/. The data set (Yan et al., 2024) is available on the figshare repository.

Acknowledgments

S.S., A.B., and C.Y. acknowledge funding from the NASA InSight Participating Scientist Program under Grant 80NSSC18K1631. A.-C.P. gratefully acknowledges the financial support and endorsement from the DLR Management Board Young Research Group Leader Program and the Executive Board Member for Space Research and Technology. A. M was funded under the SNSF Ambizione Fellowhip. C. L. J acknowledges support from the Natural Sciences and Engineering Research Council of Canada. This project was carried out at the Advanced Research Computing at Hopkins core facility (rockfish.jhu.edu) at the Hopkins High Performance Computing Center and at the Maryland Advanced Research Computing Center. This paper is InSight Contribution No. 305. The authors thank Thomas Gastine for implementing the full-sphere dynamo with code MagIC and providing valuable feedback on the manuscript. We thank two anonymous reviewers for their insightful comments that helped to improve a previous version of this manuscript and the editor Andrew Yau for handling our paper.

References

Acuna, M., Connerney, J., Ness, N., Lin, R., Mitchell, D., Carlson, C., et al. (1999). Global distribution of crustal magnetization discovered by the Mars Global Surveyor MAG/ER experiment. *Science*, *284*(5415), 790–793. https://doi.org/10.1126/science.284.5415.790

Amit, H., Christensen, U. R., & Langlais, B. (2011). The influence of degree-1 mantle heterogeneity on the past dynamo of mars. *Physics of the Earth and Planetary Interiors*, *189*(1–2), 63–79. https://doi.org/10.1016/j.pepi.2011.07.008

Andrews-Hanna, J. C., Zuber, M. T., & Banerdt, W. B. (2008). The borealis basin and the origin of the Martian crustal dichotomy. *Nature*, *453*(7199), 1212–1215. https://doi.org/10.1038/nature07011

Banerdt, W. B., Smrekar, S. E., Banfield, D., Giardini, D., Golombek, M., Johnson, C. L., et al. (2020). Initial results from the insight mission on mars. *Nature Geoscience*, *13*(3), 183–189. https://doi.org/10.1038/s41561-020-0544-y

Benjamin, P. B., Oishi, J. S., Vasil, G. M., Lecoanet, D., & Burns, K. J. (2020). Single-hemisphere dynamos in m-dwarf stars. *APJL*, *902*(L3), L3. https://doi.org/10.3847/2041-8213/abb9a4

Cébron, D., Vidal, J., Schaeffer, N., Borderies, A., & Sauret, A. (2021). Mean zonal flows induced by weak mechanical forcings in rotating spheroids. *Journal of Fluid Mechanics*, *916*, A39. https://doi.org/10.1017/jfm.2021.220

Christensen, U., Aubert, J., Cardin, P., Dormy, E., Gibbons, S., Glatzmaier, G., et al. (2001). A numerical dynamo benchmark. *Physics of the Earth and Planetary Interiors*, *128*(1–4), 25–34. https://doi.org/10.1016/s0031-9201(01)00275-8

Dehant, V., Lammer, H., Kulikov, Y. N., Grießmeier, J. M., Breuer, D., Verhoeven, O., et al. (2007). Planetary magnetic dynamo effect on atmospheric protection of early earth and mars. *Space Science Reviews*, *129*(1), 279–300. https://doi.org/10.1007/s11214-007-9163-9

Dietrich, W., & Wicht, J. (2013). A hemispherical dynamo model: Implications for the Martian crustal magnetization. *Physics of the Earth and Planetary Interiors*, *217*, 10–21. https://doi.org/10.1016/j.pepi.2013.01.001

Elkins-Tanton, L. T., Parmentier, E., & Hess, P. (2003). Magma ocean fractional crystallization and cumulate overturn in terrestrial planets: Implications for mars. *Meteoritics & Planetary Science*, *38*(12), 1753–1771. https://doi.org/10.1111/j.1945-5100.2003.tb00013.x

Elkins-Tanton, L. T., Zaranek, S. E., Parmentier, E., & Hess, P. (2005). Early magnetic field and magmatic activity on mars from Magma Ocean cumulate overturn. *Earth and Planetary Science Letters*, *236*(1–2), 1–12. https://doi.org/10.1016/j.epsl.2005.04.044

Frey, H., & Schultz, R. A. (1988). Large impact basins and the mega-impact origin for the crustal dichotomy on mars. *Geophysical Research Letters*, *15*(3), 229–232. https://doi.org/10.1029/gl015i003p00229

Greenwood, S., Davies, C. J., & Pommier, A. (2021). Influence of thermal stratification on the structure and evolution of the martian core. *Geophysical Research Letters*, *48*(22), e2021GL095198. https://doi.org/10.1029/2021GL095198

Gubbins, D. (1999). The distinction between geomagnetic excursions and reversals. *Geophysical Journal International*, *137*(1), F1–F3. https://doi.org/10.1046/j.1365-246x.1999.00810.x

Irving, J. C. E., Lekić, V., Durán, C., Drilleau, M., Kim, D., Rivoldini, A., et al. (2023). First observations of core-transiting seismic phases on mars. *Proceedings of the National Academy of Sciences*, *120*(18), e2217090120. https://doi.org/10.1073/pnas.2217090120

Jakosky, B. M., Lin, R. P., Grebowsky, J. M., Luhmann, J. G., Mitchell, D. F., Beutelschies, G., et al. (2015). The mars atmosphere and volatile evolution (maven) mission. *Space Science Reviews*, *195*(1), 3–48. https://doi.org/10.1007/s11214-015-0139-x

Jakosky, B. M., & Phillips, R. J. (2001). Mars' volatile and climate history. *Nature*, *412*(6843), 237–244. https://doi.org/10.1038/35084184

Johnson, C. L., Mittelholz, A., Langlais, B., Russell, C. T., Ansan, V., Banfield, D., et al. (2020). Crustal and time-varying magnetic fields at the insight landing site on mars. *Nature Geoscience*, *13*(3), 199–204. https://doi.org/10.1038/s41561-020-0537-x

Johnson, C. L., & Phillips, R. J. (2005). Evolution of the Tharsis region of mars: Insights from magnetic field observations. *Earth and Planetary Science Letters*, *230*(3–4), 241–254. https://doi.org/10.1016/j.epsl.2004.10.038

Ke, Y., & Solomatov, V. (2006). Early transient superplumes and the origin of the martian crustal dichotomy. *Journal of Geophysical Research*, *111*(E10). https://doi.org/10.1029/2005je002631
Khan, A., Huang, D., Durán, C., Sossi, P. A., Giardini, D., & Murakami, M. (2023). Evidence for a liquid silicate layer atop the martian core. *Nature*, *622*(7984), 718–723. https://doi.org/10.1038/s41586-023-06586-4
Khan, A., Sossi, P., Liebske, C., Rivoldini, A., & Giardini, D. (2022). Geophysical and cosmochemical evidence for a volatile-rich mars. *Earth and Planetary Science Letters*, *578*, 117330. https://doi.org/10.1016/j.epsl.2021.117330
Konopliv, A. S., Park, R. S., Rivoldini, A., Baland, R.-M., Le Maistre, S., Van Hoolst, T., et al. (2020). Detection of the chandler wobble of mars from orbiting spacecraft. *Geophysical Research Letters*, *47*(21), e2020GL090568. https://doi.org/10.1029/2020GL090568
Landeau, M., & Aubert, J. (2011). Equatorially asymmetric convection inducing a hemispherical magnetic field in rotating spheres and implications for the past martian dynamo. *Physics of the Earth and Planetary Interiors*, *185*(3), 61–73. https://doi.org/10.1016/j.pepi.2011.01.004
Landeau, M., Aubert, J., & Olson, P. (2017). The signature of inner-core nucleation on the geodynamo. *Earth and Planetary Science Letters*, *465*, 193–204. https://doi.org/10.1016/j.epsl.2017.02.004
Langlais, B., & Purucker, M. (2007). A polar magnetic paleopole associated with apollinaris patera, mars. *Planetary and Space Science*, *55*(3), 270–279. https://doi.org/10.1016/j.pss.2006.03.008
Langlais, B., Thébault, E., Houliez, A., Purucker, M., & Lillis, R. (2019). A new model of the crustal magnetic field of mars using mgs and maven. *jgrp*, *124*(6), 1542–1569. https://doi.org/10.1029/2018JE005854
Lillis, R. J., Robbins, S., Manga, M., Halekas, J. S., & Frey, H. V. (2013). Time history of the martian dynamo from crater magnetic field analysis. *Journal of Geophysical Research: Planets*, *118*(7), 1488–1511. https://doi.org/10.1002/jgre.20105
Lin, Y., Marti, P., Noir, J., & Jackson, A. (2016). Precession-driven dynamos in a full sphere and the role of large scale cyclonic vortices. *Physics of Fluids*, *28*(6), 066601. https://doi.org/10.1063/1.4954295
Marti, P., Schaeffer, N., Hollerbach, R., Cébron, D., Nore, C., Luddens, F., et al. (2014). Full sphere hydrodynamic and dynamo benchmarks. *Geophysical Journal International*, *197*(1), 119–134. https://doi.org/10.1093/gji/ggt518
Milbury, C., Schubert, G., Raymond, C. A., Smrekar, S. E., & Langlais, B. (2012). The history of mars' dynamo as revealed by modeling magnetic anomalies near tyrrhenus mons and syrtis major. *Journal of Geophysical Research*, *117*(E10). https://doi.org/10.1029/2012JE004099
Mittelholz, A., & Johnson, C. L. (2022). The martian crustal magnetic field. *Frontiers in Astronomy and Space Sciences*, *9*. https://doi.org/10.3389/fspas.2022.895362
Mittelholz, A., Johnson, C. L., Feinberg, J. M., Langlais, B., & Phillips, R. J. (2020). Timing of the martian dynamo: New constraints for a core field 4.5 and 3.7 ga ago. *Science Advances*, *6*(18), eaba0513. https://doi.org/10.1126/sciadv.aba0513
Mittelholz, A., Johnson, C. L., Fillingim, M., Grimm, R. E., Joy, S., Thorne, S. N., & Banerdt, W. B. (2023). Mars' external magnetic field as seen from the surface with insight. *Journal of Geophysical Research: Planets*, *128*(1), e2022JE007616. https://doi.org/10.1029/2022JE007616
Mohit, P. S., & Arkani-Hamed, J. (2004). Impact demagnetization of the martian crust. *Icarus*, *168*(2), 305–317. https://doi.org/10.1016/j.icarus.2003.12.005
Monville, R., Vidal, J., Cébron, D., & Schaeffer, N. (2019). Rotating double-diffusive convection in stably stratified planetary cores. *Geophysical Journal International*, *219*(Supplement_1), S195–S218. https://doi.org/10.1093/gji/ggz347
Nimmo, F., & Gilmore, M. S. (2001). Constraints on the depth of magnetized crust on mars from impact craters. *Journal of Geophysical Research*, *106*(E6), 12315–12323. https://doi.org/10.1029/2000je001325
Nimmo, F., Hart, S., Korycansky, D., & Agnor, C. (2008). Implications of an impact origin for the martian hemispheric dichotomy. *Nature*, *453*(7199), 1220–1223. https://doi.org/10.1038/nature07025
Ojha, L., Karunatillake, S., Karimi, S., & Buffo, J. (2021). Amagmatic hydrothermal systems on Mars from radiogenic heat. *Nature Communications*, *12*(1), 1754. https://doi.org/10.1038/s41467-021-21762-8
Ojha, L., & Mittelholz, A. (2023). Insight into the formation mechanism of the Medusae fossae formation on Mars from magnetic field data. *Icarus*, *395*, 115471. https://doi.org/10.1016/j.icarus.2023.115471
Pommier, A. (2018). Influence of sulfur on the electrical resistivity of a crystallizing core in small terrestrial bodies. *Earth and Planetary Science Letters*, *496*, 37–46. https://doi.org/10.1016/j.epsl.2018.05.032
Pommier, A., Davies, C. J., & Zhang, R. (2020). A joint experimental-modeling investigation of the effect of light elements on dynamos in small planets and moons. *Journal of Geophysical Research: Planets*, *125*(8), e2020JE006492. https://doi.org/10.1029/2020JE006492
Quesnel, Y., Sotin, C., Langlais, B., Costin, S., Mandea, M., Gottschalk, M., & Dyment, J. (2009). Serpentinization of the martian crust during noachian. *Earth and Planetary Science Letters*, *277*(1), 184–193. https://doi.org/10.1016/j.epsl.2008.10.012
Roberts (2007). 8.03 - Theory of the geodynamo. In G. Schubert (Ed.), *Treatise on geophysics* (pp. 67–105). Elsevier. https://doi.org/10.1016/B978-044452748-6.00133-4
Roberts, J. H., & Zhong, S. (2006). Degree-1 convection in the martian mantle and the origin of the hemispheric dichotomy. *Journal of Geophysical Research*, *111*(E6). https://doi.org/10.1029/2005je002668
Rochette, P. (2006). Crustal magnetization of mars controlled by lithology or cooling rate in a reversing dynamo? *Geophysical Research Letters*, *33*(2). https://doi.org/10.1029/2005gl024280
Samuel, H., Drilleau, M., Rivoldini, A., Xu, Z., Huang, Q., Garcia, R. F., et al. (2023). Geophysical evidence for an enriched molten silicate layer above mars's core. *Nature*, *622*(7984), 712–717. https://doi.org/10.1038/s41586-023-06601-8
Schaeffer, N. (2013). Efficient spherical harmonic transforms aimed at pseudospectral numerical simulations. *Geochemistry, Geophysics, Geosystems*, *14*(3), 751–758. https://doi.org/10.1002/ggge.20071
Schaeffer, N., Jault, D., Nataf, H.-C., & Fournier, A. (2018). Turbulent geodynamo simulations: A leap towards earth's core. *Geophysical Journal International*, *211*(1), 1–29. https://doi.org/10.1093/gji/ggx265
Solomon, S. C., Aharonson, O., Aurnou, J. M., Banerdt, W. B., Carr, M. H., Dombard, A. J., et al. (2005). New perspectives on ancient mars. *Science*, *307*(5713), 1214–1220. https://doi.org/10.1126/science.1101812
Stähler, S. C., Khan, A., Banerdt, W. B., Lognonné, P., Giardini, D., Ceylan, S., et al. (2021). Seismic detection of the martian core. *Science*, *373*(6553), 443–448. https://doi.org/10.1126/science.abi7730
Stanley, S., Elkins-Tanton, L., Zuber, M. T., & Parmentier, E. M. (2008). Mars' paleomagnetic field as the result of a single-hemisphere dynamo. *Science*, *321*(5897), 1822–1825. https://doi.org/10.1126/science.1161119
Steele, S. C., Fu, R. R., Ermakov, A. I., Citron, R. I., Lillis, R. J., & Levitt, Z. (2022). *Could weakly magnetized martian basins reflect cooling in a reversing dynamo field*. 53rd LPSC.
Steele, S. C., Fu, R. R., Volk, M. W. R., North, T. L., Brenner, A. R., Muxworthy, A. R., et al. (2023). Paleomagnetic evidence for a long-lived, potentially reversing martian dynamo at 3.9 ga. *Science Advances*, *9*(21), eade9071. https://doi.org/10.1126/sciadv.ade9071

Terasaki, H., Rivoldini, A., Shimoyama, Y., Nishida, K., Urakawa, S., Maki, M., et al. (2019). Pressure and composition effects on sound velocity and density of core-forming liquids: Implication to core compositions of terrestrial planets. *Journal of Geophysical Research: Planets*, *124*(8), 2272–2293. https://doi.org/10.1029/2019JE005936

Thomas, P., Grott, M., Morschhauser, A., & Vervelidou, F. (2018). Paleopole reconstruction of martian magnetic field anomalies. *Journal of Geophysical Research: Planets*, *123*(5), 1140–1155. https://doi.org/10.1002/2017JE005511

Vervelidou, F., Lesur, V., Grott, M., Morschhauser, A., & Lillis, R. J. (2017). Constraining the date of the martian dynamo shutdown by means of crater magnetization signatures. *Journal of Geophysical Research: Planets*, *122*(11), 2294–2311. https://doi.org/10.1002/2017JE005410

Weiss, B. P., Vali, H., Baudenbacher, F. J., Kirschvink, J. L., Stewart, S. T., & Shuster, D. L. (2002). Records of an ancient martian magnetic field in alh84001. *Earth and Planetary Science Letters*, *201*(3–4), 449–463. https://doi.org/10.1016/s0012-821x(02)00728-8

Wicht, J. (2002). Inner-core conductivity in numerical dynamo simulations. *Physics of the Earth and Planetary Interiors*, *132*(4), 281–302. https://doi.org/10.1016/s0031-9201(02)00078-x

Wilhelms, D. E., & Squyres, S. W. (1984). The martian hemispheric dichotomy may be due to a giant impact. *Nature*, *309*(5964), 138–140. https://doi.org/10.1038/309138a0

Wu, Y., Dietrich, W., & Tao, X. (2024). Parameter regimes of hemispherical dynamo waves in a spherical shell from 3d mhd simulations. *Journal of Geophysical Research: Planets*, *129*(1), e2023JE007976. https://doi.org/10.1029/2023JE007976

Yan, C., Barik, A., Stanley, S., Leung, J. S.-Y., Mittelholz, A., Johnson, C. L., et al. (2023). An ancient martian dynamo driven by hemispheric heating: Effect of thermal boundary conditions. *The Planetary Science Journal*, *4*(1), 11. https://doi.org/10.3847/PSJ/acae93

Yan, C., Barik, A., Stanley, S., Mittelholz, A., Plesa, A.-C., & Johnson, C. L. (2024). Dataset of mars hemispheric magnetic field from a full sphere dynamo [Dataset]. *figshare*. https://doi.org/10.6084/m9.figshare.25337857.v1

Zhong, S., & Zuber, M. T. (2001). Degree-1 mantle convection and the crustal dichotomy on mars. *Earth and Planetary Science Letters*, *189*(1–2), 75–84. https://doi.org/10.1016/s0012-821x(01)00345-4